BIOMICROFLUIDICS **9**, 014120 (2015)

Biomimetics of fetal alveolar flow phenomena using microfluidics

Janna Tenenbaum-Katan,[1] Rami Fishler,[1] Barbara Rothen-Rutishauser,[2] and Josué Sznitman[1,a)]
[1]*Department of Biomedical Engineering, Technion—Israel Institute of Technology, 32000 Haifa, Israel*
[2]*Adolphe Merkle Institute, University of Fribourg, 1700 Fribourg, Switzerland*

(Received 22 September 2014; accepted 23 January 2015; published online 17 February 2015)

At the onset of life *in utero*, the respiratory system begins as a liquid-filled tubular organ and undergoes significant morphological changes during fetal development towards establishing a respiratory organ optimized for gas exchange. As airspace morphology evolves, respiratory alveolar flows have been hypothesized to exhibit evolving flow patterns. In the present study, we have investigated flow topologies during increasing phases of embryonic life within an anatomically inspired microfluidic device, reproducing real-scale features of fetal airways representative of three distinct phases of *in utero* gestation. Micro-particle image velocimetry measurements, supported by computational fluid dynamics simulations, reveal distinct respiratory alveolar flow patterns throughout different stages of fetal life. While attached, streamlined flows characterize the shallow structures of premature alveoli indicative of the onset of saccular stage, separated recirculating vortex flows become the signature of developed and extruded alveoli characteristic of the advanced stages of fetal development. To further mimic physiological aspects of the cellular environment of developing airways, our biomimetic devices integrate an alveolar epithelium using the A549 cell line, recreating a confluent monolayer that produces pulmonary surfactant. Overall, our *in vitro* biomimetic fetal airways model delivers a robust and reliable platform combining key features of alveolar morphology, flow patterns, and physiological aspects of fetal lungs developing *in utero*. © *2015 AIP Publishing LLC*. [http://dx.doi.org/10.1063/1.4908269]

I. INTRODUCTION

Human lungs undergo significant morphological changes during prenatal development *in utero*. Lung buds evolve to form a tubular tree, rapid branching devises structured airways, and septation dramatically expands the surface area of lung parenchyma.[1] Taken together, anatomical changes transform the pulmonary tree from a "tubular organ" to one ultimately designed for optimized gas exchange;[2,3] that is, a space-filling tree with more than 100×10^6 pulmonary alveoli.[4,5] Two morphological and physiological requirements are essential to this end:[1,2,6] (i) maximizing the pulmonary surface area in contact with alveolar capillaries and (ii) developing a functional air-blood barrier at the alveolar wall. While the former is only fully accomplished after birth,[7,8] the latter is guaranteed by differentiation of the continuous alveolar epithelium lining, a cellular process initiated in the canalicular gestational stage (∼16–26 weeks). By the end of this developmental phase, the epithelium represents a cellular mosaic constructed of type I alveolar epithelial cells (AEC I) that form the basic structure of the alveolar wall and importantly, secretory type II cells (AEC II) that are indispensable to proper physiological functionality of the alveolar environment.[1] Not only do AEC II act as progenitors to AEC I[9] and contribute to innate defence mechanisms,[10] they critically secrete pulmonary surfactant that reduces

a)Author to whom correspondence should be addressed. Electronic mail: sznitman@bm.technion.ac.il

surface tension at the air-liquid interface after birth.[11,12] Overall, differentiated and surfactant-secreting AEC II represent a strong manifestation of the alveolar air-blood barrier and thus, a milestone towards feasible gas exchange.[1] Given their underlying role during fetal development, understanding respiratory maturation towards *ex utero* life requires a comprehensive assessment of the physiological factors influencing AEC II functionality.

Among the acknowledged factors, mechanical forces represent an important regulator of both structure and function of the alveolar epithelium.[13] To this end, there has been a growing interest in the role of mechanical strain on AEC II;[14] past studies have demonstrated how stretch stimuli influence, for example, both surfactant secretion[12,15–17] and epithelium permeability.[18] *In utero*, mechanical strain experienced by the embryonic epithelium results from spontaneous expansion and contraction motions known as fetal breathing movements[19] (FBMs) that are evocative of healthy fetal life;[20–22] FBMs induce constant cyclic strains on the parenchyma that promote maturation of the epithelium.[15,19] Since fetal lungs develop as a liquid-filled organ, a notable consideration are the associated fluid displacements resulting from lung liquid volume changes during FBMs;[23] these flows generate small, yet finite wall shear stresses (WSSs) on the submerged embryonic alveolar epithelium. To date, investigations of WSS on AECII have been mostly driven by considerations of cell injury and damage caused by liquid plug propagations along airways;[24–26] only recently has the role of WSS begun attracting attention in the context of surfactant secretion.[27] Hence, despite ongoing progress in uncovering physiological responses of AECII to mechanical and flow-induced stimuli, few if any studies have addressed AECII function in the context of the significant morphological changes that arise *in utero* during fetal lung development.

Morphological changes in embryonic lungs are known to give rise to a structural diversity of airway shapes during prenatal development. To begin, shallow indentations of airway ducts highlight the formation of primitive alveoli that are recognizable as early as 29 weeks of gestation.[28,29] These cavities gradually evolve through the septation process and develop into deep, hollow cavities,[30] where topological changes spanning primitive alveoli to developed airspaces may be quantified by measuring a characteristic alveolar depth,[28,31,32] or radius (R), and an alveolar mouth opening length (L); the two of which can be related[33] through an alveolar mouth half-opening angle, $\alpha = \sin^{-1}(L/2R)$, shown in Fig. 1(a). Such changes have been hypothesized to influence respiratory alveolar flow patterns and determine whether attached or recirculating flows reside within fetal alveolar cavities,[34,35] embodying the different phases of embryonic development. Until present, however, studies on the evolution of alveolar flow phenomena in relation to fetal alveolar development have been solely limited to Computational Fluid Dynamic (CFD) simulations for inhaled drug delivery in infants,[36] with little or no knowledge on their possible effects on AEC II function.

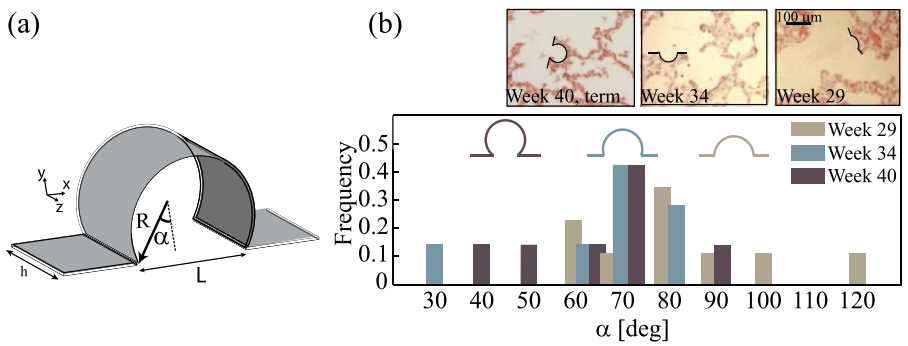

FIG. 1. (a) Schematic of the half mouth-opening angle, α, quantifying topological characteristics of alveolar cavities. (b) Normalized frequency distribution of α throughout developing fetal airways. Data estimated from micrographs of histological samples of prenatal lungs (insets), capturing topological changes of alveolar spaces occurring during development of fetal lungs. Three representative values of α were chosen to exemplify 3 phases of lungs *in utero*; spanning the period from week 29 (onset of emerging alveoli) to week 40 (expected term of delivery). Reproduced with permission from Hislop, J. Anat. **201**(4), 325–334 (2002). Copyright 2002 Wiley Online Library.

Motivated by this dearth of knowledge, we attempt in the present work to shed some light on the intricate coupling that arises between alveolar morphology, flow phenomena, and AEC II function during fetal lung development. To this end, we utilize microfluidic-based biomimetic analogs of the fetal alveolar environments, representative of distinct fetal stages. In recent years, microfluidic devices have become attractive platforms to investigate respiratory physiology using cellular *in vitro* environments of lung airways.[26,37–39] By combining experimental micro-Particle Image Velocimetry (μPIV) measurements within our microfluidic devices with numerical (CFD) simulations, and finally integrating a human alveolar epithelium (A549 cell line), we present a systematic investigation of AEC II function, including epithelium integrity and surfactant secretion, which sheds new light on physiologically relevant alveolar flow patterns representative of the developing fetal lungs.

II. METHODS

A. Anatomically inspired microfluidic device

As a first approximation, morphological changes of fetal alveolar sacs are captured by decreasing values of the mouth half-opening angle, α. To span sequential developmental phases of fetal airspaces, three representative values of α were chosen (Fig. 1(b)), following image analysis of micrographs obtained from histological samples of the alveolar airspaces (Fig. 1(b), inset); such histological sections were taken at increasing stages of human fetal lung development, namely, at 29, 34, and 40 weeks of gestation.[28,29] The measured values of α from image analysis cover a wide range of cavities, from 120° to 30°, that feature extremely shallow geometries to highly extruded spherical-like cavities. We capture this broad spectrum of angles with 3 representative values ranging from $\alpha \approx 100°$ to $\alpha = 45°$, characterizing an extreme value of the half-opening angle; in particular, this latter value is close to that frequently used ($\alpha = 60°$) to model fully developed adult alveoli.[33] To guide the reader with time points during gestational stages of fetal development, we associate the chosen values of α (i.e., 97°, 68°, and 45°) throughout the text as 29, 34, and 40 weeks of gestation, namely, from the appearance of the first alveolar cavities[28] to the term of birth. In turn, our anatomically inspired design reproduces distinct phases of fetal alveolar development.

Standard soft-lithography techniques[27,40] were used to fabricate a poly(dimethylsiloxane) (PDMS) microfluidic-device modeling pulmonary structures and respiratory features at realistic, true one-to-one- anatomical scales.[2,28] Our model combines straight channels (i.e., $w = 400\,\mu$m in width and $h = 100\,\mu$m in height) with cylindrical cavities ($R = 40\,\mu$m in radius), modeling fetal airway ducts in combination with alveolar airspaces (Figs. 2(a) and 2(b)), where the underlying geometry of evolving fetal alveolar spaces is captured by the varying values of α (see Figs. 2(c)–2(e)). Since microcavity flow patterns are known to be influenced by cavity depth as well as mouth opening angles,[41] two fixed cavity depths (h) were assumed to approximate the range of *in vivo* values of the alveolar space, where we screened in our microfluidic models values of the dimensionless ratio spanning $R/h = 0.4$–0.6; note that $R/h = 0.5$ would correspond to a sphere.

B. Quantitative particle image velocimetry measurements

Quantitative characterization of fetal alveolar flow patterns were obtained using microparticle image velocimetry (μPIV) across the midplane of the alveolar cavities, following recent experiments for low-Reynolds-number microfluidic cavities.[41] Briefly, polystyrene red fluorescent beads ($d = 0.86\,\mu$m) were suspended in a 60% (v/v) glycerol solution in water and flown through the device using a syringe pump at a fixed $Re = 0.1$; such value is within the physiological range of anticipated alveolar fetal flows (see Sec. II C and supplementary material[76]). Here, the Reynolds number is defined as $Re = \frac{\bar{U} D_h}{\nu} = \frac{2Q}{(h+w)\nu}$, where D_h is the hydraulic diameter, $\bar{U} = \frac{Q}{w \times h}$ is the average velocity in the duct, Q, the flow rate imposed by the syringe pump (i.e., perfusion rate, see Sec. II C), and ν is the kinematic viscosity of the fluid.

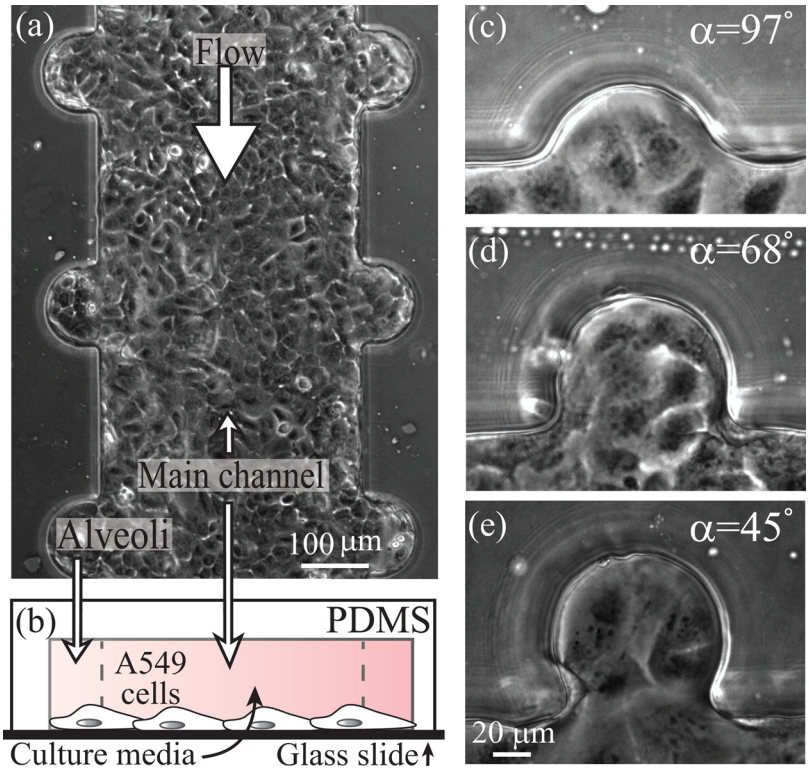

FIG. 2. Anatomically inspired microfluidic model of airways developing *in utero*. (a) Phase-contrast image of a microfluidic device combining straight ducts (resembling airways) with cylindrical cavities (mimicking alveolar spaces) lined with a confluent monolayer of A549 cells, a model of alveolar epithelium. (b) Schematic cross-section illustrating the combination of duct and cavities. (c)–(e) Phase-contrast image of selected values of α, representative of increasing stages of fetal airways, scale bar specified in (e).

Image sequences of the steady-state flow were captured using fluorescence microscopy at 20× magnification; two-dimensional (2D) velocity fields were obtained for each alveolus using a PIV sum-of-correlation algorithm on 100 consecutive images,[41,42] with a final interrogation window size of 32 pixels and 50% overlap, resulting in a spatial resolution of approximately 4.6 μm. Due to the large range of velocity magnitudes characterizing the alveolar flow topology, only a sub-region of the flow field could be resolved using a single frame rate. Hence, for each alveolar cavity, experiments were repeated using different frame rates (i.e., 50–1000 frames/s), and a full flow map was subsequently reconstructed by averaging overlapping data points.

C. Microfluidic cell culture

Human type II alveolar epithelial cells (A549) (American Type Culture Collection, ATCC, Biological Industries) were cultured in RPMI-1640 medium with L-glutamine (Sigma) supplemented with 10% FBS (Biological Industries) according to established protocols;[27] the A549 cell line is a well-characterized and widely used *in vitro* lung epithelial model for human alveolar type II-like cells.[43–45] Briefly, microfluidic devices were treated with 0.01% collagen (from rat tail, type I, Sigma) at 37 °C for 1 h, exposed to ultraviolet (UV) light and cultured with the A549 cell line at a seeding density of 1×10^6 cells/ml at a total volume of 45 μl. Devices were left for 30 min at steady environmental conditions of 5% CO_2 and 37 °C to let cells properly adhere and were further kept under constant perfusion of fresh media, until confluent monolayers are attained (Figs. 2(a) and 2(c)–2(e)). Following a classic symmetric and dichotomously branching airway model,[46] in association with experimental measurements collected from human fetal airways,[28,47,48] continuous perfusion of our cultured microfluidic channels was chosen to match estimated *in vivo* conditions in terms of flow perfusion velocities, associated

Reynolds number (Re), and representative WSSs acting on the alveolar epithelium (see supplementary material[76] for further details and derivation). To meet such requirements perfusion rates through the main channel were chosen at 1 μl/min, corresponding to $Re = 0.1$, an average wall shear stress value of $\tau = 0.17$ dyn/cm^2 on the epithelium (i.e., bottom apical surface of the channel) and a velocity of 4×10^{-4} m/s within our main channel. Note that such perfusion rate matches not only *in vivo* estimated values,[28,47,48] but is also acknowledged to deliver an efficient growth rate and proliferation of A549 cells cultured within microfluidic devices.[49]

D. Immunofluorescence and confocal imaging

To examine the production of pulmonary surfactant, A549 cells were fluorescently marked for lamellar bodies[27,38] (LBs). Cells were loaded with 1 μM quinacrine (Sigma), a fluorescent marker of LBs, for 40 min at 37°. Images were acquired using an inverted epi-fluorescent microscope (Nikon Ti-E). Epithelial integrity and monolayer formation were examined with laser scanning microscopy (LSM) by means of F-actin filaments distribution of cultured A549 cells. Cells were fixed with 4% paraformaldehyde for 15 min, permeabilized with 0.5% triton X-100 (Sigma) in PBS for 5 min at 4 °C, followed by labelling with rhodamine-phalloidin (50 μg/ml, Sigma) and DAPI (Sigma) for 40 min at room temperature for Actin and Nuclei, respectively. Samples were examined using an LSM (LSM 710, Carl Zeiss Inc.) and 3D images were constructed from the acquired Z-stacks using Imaris software (Bitplane AG, Zuürich, Switzerland).

E. Image analysis

Production of LBs by A549 cells was determined by quantifying the area of fluorescently marked LBs[27] out of the entire area occupied by the cells examined. Using ImageJ software, fluorescent images of LBs within alveolar cavities were converted to binary masks and the total area of stained LBs was extracted. These extracted data were converted to a percentage of area occupied by LBs within the cells of interest, by determining a ratio of total LB area to the surface area populated by cells in each examined cavity; the latter was assessed using phase-contrast images of regions of interest (ROI). Overall, we estimated and compared the extent of LB production by A549 cells in each examined cavity and general ROIs situated within the main duct. A non-parametric rank sum statistical test was used to examine the statistical significance of our data.

F. Computational fluid dynamics

Numerical solutions of the steady-state three-dimensional (3D) flow field were obtained as previously reported.[41] Briefly, finite-element simulations of the Navier-Stokes for incompressible flow equations were performed using a commercially available software (COMSOL Multiphysics, version 4.3b). The geometrical parameters characterizing each alveolus simulated (including R, α, h, and w) were chosen to match with high fidelity the geometry of the microfluidic devices as measured from image analysis. Tetrahedral mesh elements were used to mesh the domain leading to a total of 1.3×10^6 to 2.2×10^6 mesh elements, depending on the specific alveolar cavity simulated. Fluid properties were selected to match those of water at 37° ($\nu = 6.78 \times 10^{-7}$ m^2/s), and a laminar velocity profile was imposed at the inlet of the channel.

Dynamic similarity between experiments and simulations was achieved by imposing the appropriate flow rate, Q, to match experimental flow conditions of $Re = 0.1$ in the central channel. A constant pressure of 100 000 Pa was arbitrarily set at the domain outlet.[33,50,51] Mesh refinement studies were performed to ensure that flow solutions were grid independent where changes in the average flow velocity magnitude and average shear rate over the alveolar cavity opening were within 1% upon further mesh refinement, as previously established.[41] All numerical solutions were found to converge with residuals below 10^{-7}, measuring the imbalance in conservation of mass.[52] Velocity fields and corresponding WSSs were subsequently extracted at the bottom alveolar wall, parallel to the x-y plane (as defined in Fig. 1(a)).

III. RESULTS AND DISCUSSION

A. Fetal alveolar flow patterns

Alveolar flow patterns characteristic of the developing airspaces are qualitatively shown in Fig. 3 (left column) using reconstructed steady-state streaklines (i.e., streamlines), where images are obtained by continuously re-estimating at each image pixel the mean intensity value over a sequence of 50–100 consecutive frames; flows are shown for different α values at a fixed cavity depth of $R/h = 0.4$ (see Fig. S1 in the supplementary material[76] for corresponding results at $R/h = 0.6$). As the alveolar cavity is gradually extruded away from the duct (i.e., decreasing α), alveolar flow patterns change sensibly from an attached flow configuration (Fig. 3(a), Multimedia view) to separated flow with a single recirculation zone (Figs. 3(b) and 3(c), Multimedia view). Here, we note that values of α influence the location of the vortex centre, where higher values correspond qualitatively to a vortex core positioned closer to the duct (compare Figs. 3(b) and 3(c); left column), underlining the topological flow changes occurring during gestational stages *in utero*.

To capture more quantitatively alveolar flow changes occurring *in utero*, Fig. 3 (second column) presents normalized velocity magnitudes, $|\boldsymbol{u}^*|$ (and corresponding streamlines) along the *x-y* midplane of alveolar cavities (Fig. 1(a)), as measured by μPIV. Here, we define $|\boldsymbol{u}^*| = |\boldsymbol{u}/\bar{U}|$, where $\boldsymbol{u}$ is the 2D projection of the velocity field along the *x-y* mid-plane. While attached flow ($\alpha = 97°$) is characterized by velocity magnitudes that are similar to (or approximately an order of magnitude less than) those measured in the alveolar duct (Fig. 3(a)), separated alveolar flows result in contrast to a velocity drop of at least two orders of magnitude relative to the duct (Figs. 3(b) and 3(c)); this latter flow characteristic is a well-known property of low-*Re* separated cavity flow phenomena[34,41,53,54] and has been previously shown in the context of adult air-filled lungs both experimentally[41,55,56] and numerically.[33,51,57,58]

To deliver a comprehensive rendering of the different flow regimes anticipated across the developmental stages of fetal lungs, our numerical and experimental flow results are summarized in the phase map of Fig. 4. Namely, fetal alveolar flow regimes and topologies can be predicted as a function of the relative cavity depth (R/h) and mouth half-opening angle (α). Our *in vitro* microfluidic results highlight that varying flows regimes are anticipated to be

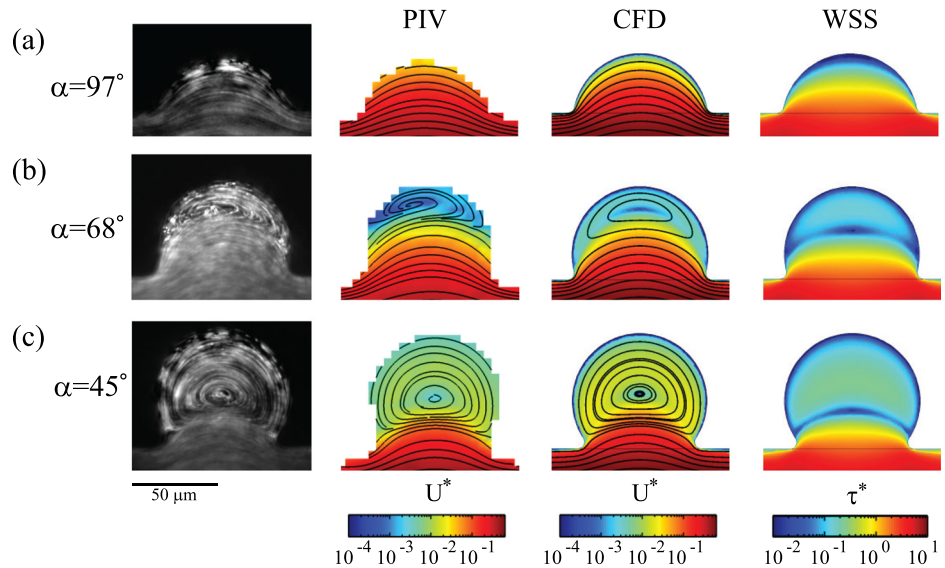

FIG. 3. Characteristic flows within fetal alveolar cavities through development *in utero*. Flow patterns change from attached (a), to separated flow with a single recirculation zone (b)–(c). Left to right: results correspond to qualitative flow visualizations (i.e., steady-state streaklines), μPIV, and CFD simulations, respectively. WSS simulations (right-hand column) show near-zero shear stress environment experienced by epithelial cells within alveolar cavities. Both velocity fields and WSS are shown normalized (see text for details). All experiments were performed matching $\mathrm{Re} = 0.1$. Videos are slowed down by a factor of 10. (Multimedia view) [URL: http://dx.doi.org/10.1063/1.4908269.1] [URL: http://dx.doi.org/10.1063/1.4908269.2] [URL: http://dx.doi.org/10.1063/1.4908269.3]

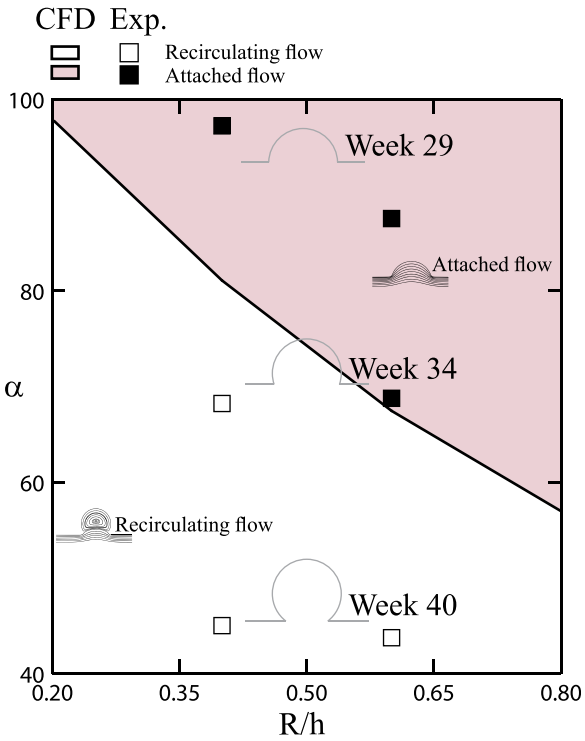

FIG. 4. Phase diagram of alveolar cavity flow patterns, combining numerical simulations and experimental results. Flow configurations are presented according to varying geometrical parameters, i.e., half mouth opening angle (α) and cavity depth (R/h). Patterns of flow sensibly change during the development of fetal airspaces; illustrating both attached (weeks 29–34 of Gestation) and separated recirculating (weeks 34–40) flow configurations and a cross-over region between the two regimes.

experienced by the alveolar epithelium lining the airspace as flow patterns evolve from attached during early developmental phases to recirculating in more mature-like alveoli, with the emergence of a cross-over period from one regime to the other.

B. Fetal alveolar wall shear stresses

Since WSS acting upon AEC II is acknowledged to influence regulated pathways of surfactant secretion, as well as distribution of actin filaments within A549 cells,[27] we have sought to quantify WSS exerted on the epithelium to account for finite shear stresses emerging *in utero*, as a result of FBMs. Here, we have used numerical simulations (see Sec. II F) to calculate the estimated WSS exerted on the bottom channel surface since direct WSS measurements are not straightforwardly obtainable. We note that although the exact cell thickness of the epithelium was neglected in our simulations, our values provide as a first approximation a reasonable estimate[59] of the WSS values the epithelium may be experiencing. We emphasize again that our computational simulations (Fig. 3, third column) were compared with both streamline patterns and corresponding velocity magnitudes along the midplane of the geometry obtained experimentally by μPIV (Fig. 3, second column), where we find generally good qualitative agreement. Although velocities obtained experimentally are slightly lower compared with CFD, the agreement remains close locally within the alveolar cavities. Note that the most significant differences are observed within the duct, with a factor up to approximately two; these discrepancies[41] are thought to be due to inaccuracies in evaluating the mean ductal velocity based on the flow rate from the syringe pump (Q) and the duct dimensions (w and h), as well as the depth of correlation in our micro-PIV setup ($\sim$16 μm).

As noted earlier (see Sec. II C and supplementary material[76]), WSS magnitudes experienced in the main channel are on the order of $\tau = 0.2$ dyn/cm^2. Following the flow topologies observed

inside microfluidic alveoli, numerical results highlight WSS values that span 1 to 2 orders of magnitude lower than in the central duct (Fig. 3, last column); this is particularly true within more extruded alveolar cavities, characteristic of later gestational stages. Our results highlight that at the onset of alveolar flow recirculation during fetal development the flow separation line (Figs. 3(a) and 3(b); last column), known as the separatrix,[57] gives rise to a thin region of near-zero WSS such that the epithelium residing within alveolar cavities becomes rather isolated in a near-zero WSS environment in contrast to the epithelium lining the main duct. As low values of flow and shear rate might affect the physiological conditions of cells by confining oxygen and nutrients transport,[60,61] we have undertaken to examine (see below) several aspects of both general cellular physiology and specific features relevant to alveolar development in relation to the substantial morphological changes occurring at the alveolar level of the developing lungs.

C. Biomimetics of *in utero* fetal lungs

As shown in Figs. 2(a) and 2(c)–2(e), our microfluidic model mimics both alveolar spaces and air ducts where confluent layers of A549 cells are obtained after up to 3 days in culture across all investigated cavities as well as in the central duct. This epithelial lining represents an uninterrupted layer of cells, emulating an intact epithelium, an essential aspect of gas exchange surfaces at developing, and adult human lungs.[1,4] Furthermore, our results indicate that neither confluency (Figs. 2(a) and 2(c)–2(e)) nor viability (see Fig. S2 in the supplementary material[76]) of the epithelial sheet are potentially jeopardized under different local alveolar flow regimes (i.e., attached flow versus separated recirculation) and corresponding low flow velocities and WSS magnitudes; such outcome is important since various flow chambers (e.g., bioreactors) and specifically microfluidic perfusion systems are known to influence cell cultures by means of varying shear stresses.[61,62] Overall, our biomimetic devices exhibit A549 cells that are growing to the typical epithelium appearance in the microfluidic system across all representative gestational lung stages.

To further assess significant aspects of the alveolar epithelial lining, we have examined two main features of our cultured cells: (i) the formation of a confluent monolayer by the epithelial lining as alveolar cells coat the airway walls with a thin single layer of cells, and (ii) the presence of LBs, characteristic organelles containing surfactant in alveolar epithelium;[12] this latter property is an inevitable aspect of lung maturation featuring the production and secretion of pulmonary surfactant by type II epithelial cells.

Using confocal microscopy, we have inspected the epithelial lining in our microfluidic device to estimate monolayer formation (Fig. 5); namely, A549 cells creating a thin coating, mimicking delicate structures of alveolar epithelium. Here, our observation of uniformly distributed F-actin (Fig. 5, green) is yet another indication of the robustness of cultured cells in parallel to cell nuclei (Fig. 5, white) presenting various stages of the cell cycle.

Using fluorescence markers, we have examined the production of pulmonary surfactant within cultured cells. A549 cells present distinct appearances of LBs (Fig. 6(a), inset) indicating continuous production of surfactant, as observed in such alveolar epithelial model cells. Namely, we have found no significant differences between surfactant production across the varying alveolar topologies (Fig. 6(b)), indicating a functional model of AEC II throughout all inspected alveolar cavities.

Overall, the findings detailed above emphasize that our microfluidic design provides a robust and attractive biomimetic model of developing fetal airways *in utero*.

D. Discussion and limitations

In the present work, we have designed and manufactured an *in vitro* microfluidic platform that to the best of our knowledge reproduces for the first time alveolar structures during prenatal life *in utero*. In particular, our efforts are aimed at delivering a platform that is robust, reproducible, and easy to manufacture. Despite such accomplishments, we still face, however, a number of limitations in reproducing a cellular environment that mimics faithfully the alveolar epithelium *in vivo*. To begin, by the end of the canalicular stage *in utero* (26 weeks of

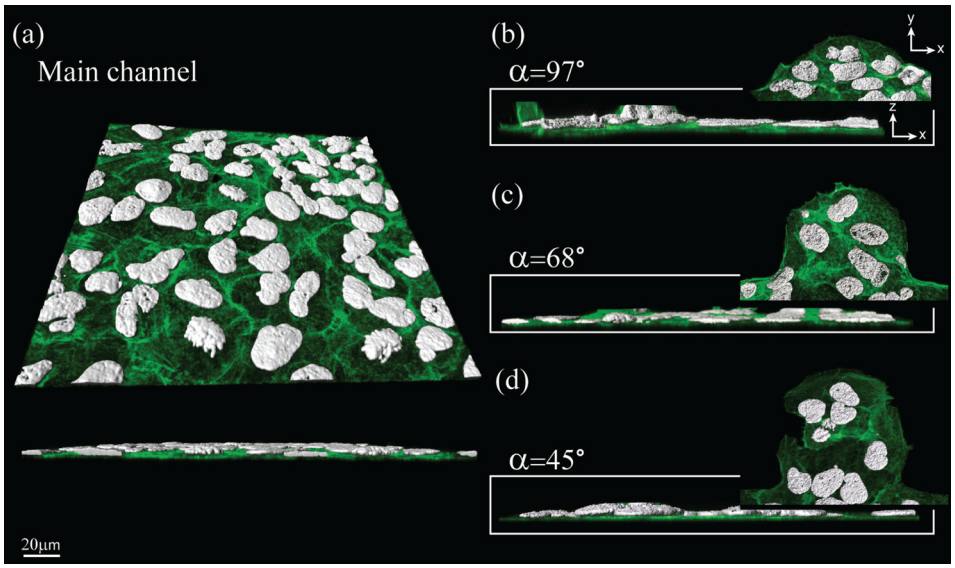

FIG. 5. Confocal images of A549 cells within microfluidic channels. Well-distributed F-actin filaments (green) are observed along the x-y plane throughout the varying geometries shown in (a)–(d); a distinct monolayer layer of cells can be shown along the x-z plane. Cell nuclei (white) present various stages of the cell cycle, indicating the healthy condition of the cells within all cavities (b)–(d) as well as in the main channel (a). The images represent minimal intensity projections for the green channel (F-actin) with an overlay of surface rendering for the white channel (cell nuclei).

gestation), the epithelium is differentiated and gathers a mosaic of types I and II alveolar cells.[1] Hence, a model incorporating a single cell type (i.e., A549 cells) is fundamentally inaccurate compared to the *in vivo* epithelium.[63,64] Having said that, to date, some of the most widely used cell culture *in vitro* models of the lungs are in fact still designs incorporating a single type of cells.[63,65] Although extensive work has been invested in developing more realistic *in vitro* environments of the epithelial barrier,[43,63,65] these efforts have been overwhelmingly limited to standard well culture systems.

To date, state-of-the-art microfluidic environments of alveolar airways exclusively model the epithelium with a single cell type culture, most commonly the A549 cell line.[26,38,39,66,67] The A549 cells have been shown to produce and release surfactant proteins[68] and belong to the most widely used *in vitro* models in lung research.[64] Only recently, a rare few microfluidic examples have attempted to integrate instead alveolar primary cells;[69,70] however, such systems still require highly intricate fluidic schemes in order to provide the necessary support for such delicate cellular environments. Another limitation for the use of primary cells is that they represent a rather heterogeneous population of different cell types, since each isolation is unique and

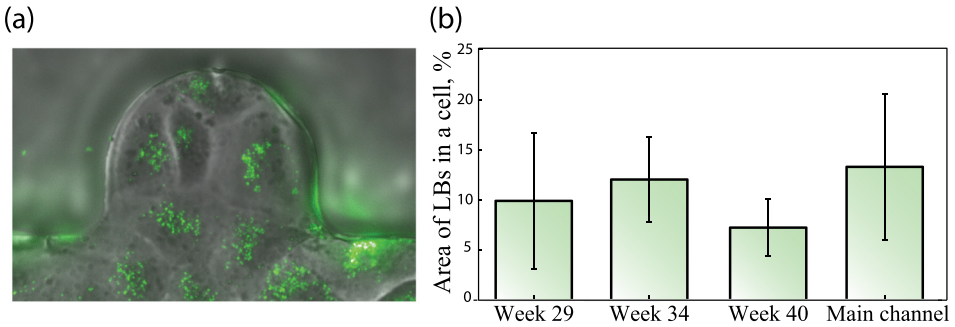

FIG. 6. (a) Fluorescently marked LBs were used to assess production of pulmonary surfactant by A549 cells within alveolar cavities and the main duct. (b) Notable presence of LBs supports continuous production of pulmonary surfactant, with no statistically significant difference between all cavities and the main channel. A non-parametric rank sum statistical test was used to examine statistical significance between 4 groups ($n = 5$–11).

impossible to exactly reproduce. The limited number of cells which can be received during each isolation, and an uncertainty due to donor variation also represents a big disadvantage.[71] Undoubtedly, further reconstruction of realistic epithelial barrier functions, including but not limited to immune cells, is of high importance when considering, for example, pharmaceutical research and cytotoxicity[72] aspects, such as those involved in the translocation processes of deposited particles across the air-blood barrier.[70,73] Here, we have presented a microfluidic device designed to model several developmental stages of fetal airways, where further enhancements of our model will be sought in the future to address some of the aforementioned scientific questions in relation to epithelial barrier functions.

With respect to flow considerations, since our biomimetic model examines the effects of geometrical variations on flow characteristics within fetal alveoli alongside with physiological aspects of the alveolar epithelium, we note that minor changes in the alveolar geometry may potentially lead to significant alternations in ensuing flow patterns (see Fig. 4, in the vicinity of the cross-over region between attached and recirculating flows). Indeed, it is well known that for low-Reynolds-number flows (i.e., Stokes' flows), cavity flow topologies are sensitive to the exact geometrical configuration[41] (see also further discussion in the supplementary material[76]). Following such considerations, we have examined both in simulations and experiments two representative values of cavity depth, i.e., both $R/h = 0.4$ (shown here) and $R/h = 0.6$ (shown in Fig. S1 in the supplementary material[76]) demonstrate that flow topologies are very similar for the two aspect ratios investigated. However, at $R/h = 0.6$ the transition from attached to recirculating flow occurs at a lower value of α, which would correspond to a slightly later stage during gestation (Fig. 4). Despite the inherent sensitivity of flow patterns to geometry under low *Re* flow conditions, we have nevertheless shown that critical physiological aspects of A549 cells are not hindered by flow separation and maintain functionality even under an isolated, near-zero WSS environment (see Figs. 5 and 6), where we recall that the estimated *in vivo* aspect ratio for fetal airways would lie closest to $R/h = 0.5$.

When discussing alveolar cavities, one must recall the distinct physiological structure of dense airspaces tightly populating airway ducts.[74] Our microfluidic designs feature instead spacious cavities populating a straight channel (Fig. 2(a)) that are not entirely faithful to *in vivo* conditions. Note, however, that we have chosen here to focus, both experimentally and computationally, on characteristic isolated alveolar geometries to examine solely flow phenomena occurring within single alveoli, despite the potential influence of neighboring alveoli. Namely, in the context of adult *ex utero* lungs it has been shown in numerical simulations that dense alveoli sharing inter-septal walls do not sensibly influence flow patterns in the depths of alveolar cavities,[51,58] such that we do not anticipate fetal alveolar flow patterns resolved here to be changed sensibly. Furthermore, our examination of micrographs (see Fig. 1(b)) taken at various developmental fetal phases[28,29] show that during gestation alveoli are relatively spread inside the pleural space as opposed to densely occupying the parenchymal space (i.e., adult stage); this latter observation is indeed anticipated, since the majority of the alveolarization process occurs postnatally.[7,8]

As pulmonary flows *in vivo* result from parenchymal expansion and contraction motions (i.e., FBMs), the fetal alveolar epithelium is anticipated to sense bi-axial flows and shear stresses that change during the breathing cycle. In the present model, we have opted for uniaxial flow conditions under the assumption that such unsteady, oscillatory effects are negligible as a first approximation. Namely, small tidal volume changes during fetal breathing movements[19] ($\sim$2%), and consequently even smaller linear displacements of the alveolar walls during FBMs (strains $< 1\%$, see supplementary material[76]), support our assumptions; computational simulations of a breathing cycle with wall motion show that flows in the developing airspaces maintain a qualitatively similar pattern between oscillatory flows and steady-state conditions (Fig. S3, see supplementary material[76]). While our experiments do not directly answer whether flow reversibility could potentially influence cellular physiology (e.g., surfactant secretion), we note that small (sub-unity) values of the dimensionless Womersley number ($Wo \ll 1$) across fetal developmental stages (see supplementary material[76]) underline that fetal alveolar flows are

inherently quasi-steady.[34] In other words, alveolar flow topologies will remain unchanged throughout FBMs and are not anticipated to markedly affect such physiological processes.

Finally, it is stressed here that the planar quasi-3D geometry of our microfluidic devices (see supplementary material[76]) should not be confused with 2D flow configurations, where no out-of-plane flows exist. Indeed, the present alveolar cavities yield intricate 3D flow structures.[41] Although confocal micro-PIV measurements have the potential to resolve such 3D flow structures,[75] given the imaging limitations of our micro-PIV setup which is restricted to a volume illumination, we have discussed here only 2D flow field measurements of projections along the midplane of the alveolar geometry. Despite such velocimetry limitations, it is important to note that our 3D cellular imaging analysis was conducted on the alveolar epithelium using confocal microscopy (see Fig. 5). Furthermore, omitting for the small thickness of the epithelium ($<5\%$ of the channel height), the estimated wall shear stresses exerted on the epithelial carpet are extracted from computational simulations using geometries identical to those microfabricated, thus giving reasonable first estimates of the WSS anticipated in the *in vitro* microfluidic environment.

IV. CONCLUSIONS

We have presented an anatomically inspired microfluidic design that mimics alveolar regions during increasing stages of fetal lung development. Our designs reproduce, at a true scale, characteristic features of developing airspaces starting as shallow indentations and gradually forming more spherical-like cavities portraying developed alveolar spaces. We have combined numerical simulations (CFD) and microfluidic experiments to unveil the range of flow patterns anticipated to characterize developing phases of fetal lung life. By integrating an A549 cell line to model the epithelium lining alveolar regions of the lung, we reconstitute a healthy confluent monolayer mimicking a thin layer of cells lining the airway lumen and featuring production of pulmonary surfactant throughout all alveolar cavities examined. Altogether, to the best of our knowledge we demonstrate for the first time a robust, biomimetically relevant and applicable design capturing morphological changes, varying flow patterns, and physiological aspects that are anticipated to occur during the development of fetal lungs *in utero*. Furthermore, with such developed platform, we have demonstrated and hypothesized a window of time during gestation when alveolar cavity flows are anticipated to evolve from attached to a separated configuration. Such microfluidic platform may be leveraged for further *in utero* respiratory physiology studies.

ACKNOWLEDGMENTS

The authors would like to thank Dr. Limor Minai (Technion, Israel), Dr. Sanjeev K. Mahto (Indian Institute of Technology, Banaras Hindu University, Varanasi, India), and Dr. Olga Kossover (Technion, Israel) for helpful discussions on microfluidics and cell biology. The support from Dr. Dimitri Vanhecke (AMI, University of Fribourg) for the LSM pictures is acknowledged. This work was supported in part by the European Commission (FP7 Program) through a Career Integration Grant (PCIG09-GA-2011-293604), as well as by the Israel Science Foundation (ISF Grant No. 990/12), and a Research Grant Award No. PGA 1302 from the Environment and Health Fund (EHF), Israel. The authors acknowledge support from the Nevet grant program of the Russel Berrie Nanotechnology Institute (RBNI, Technion). Microfabrication was conducted at the Micro-Nano fabrication Unit (MNFU, Technion).

[1]J. C. Schittny and P. H. Burri, *Fishmans Pulmonary Diseases and Disorders* (2008), pp. 91–114.
[2]E. R. Weibel, B. Sapoval, and M. Filoche, Respir. Physiol. Neurobiol. **148**, 3 (2005).
[3]E. R. Weibel, Eur. Respir. J. **31**, 483 (2008).
[4]E. R. Weibel, *The Pathway for Oxygen: Structure and Function in the Mammalian Respiratory System* (Harvard University Press, 1984).
[5]M. Ochs, J. R. Nyengaard, A. Jung, L. Knudsen, M. Voigt, T. Wahlers, J. Richter, and H. J. G. Gundersen, Am. J. Respir. Crit. Care Med. **169**, 120 (2004).
[6]D. Massaro and G. D. Massaro, Am. J. Physiol. **282**, L345 (2002).
[7]M. S. Dunnill, Thorax **17**, 329 (1962).

[8]P. H. Burri, Annu. Rev. Physiol. **46**, 617 (1984).
[9]H. Fehrenbach, Respir. Res. **2**, 33 (2001).
[10]P. Gehr, F. H. Y. Green, M. Geiser, V. I. Hof, M. M. Lee, and S. SchüRch, J. Aerosol Med. **9**, 163 (1996).
[11]C. B. Daniels and S. Orgeig, News Physiol. Sci. **18**, 151 (2003).
[12]A. V. Andreeva, M. A. Kutuzov, and T. A. Voyno-Yasenetskaya, AJP Lung Cell. Mol. Physiol. **293**, L259 (2007).
[13]A. J. Banes, in *Physical Forces and the Mammalian Cell* (Academic Press, 1993), p. 81.
[14]E. Roan and C. M. Waters, Am. J. Physiol. **301**, L625 (2011).
[15]J. Sanchez-Esteban, L. A. Cicchiello, Y. Wang, S.-W. Tsai, L. K. Williams, J. S. Torday, and L. P. Rubin, J. Appl. Physiol. **91**, 589 (2001).
[16]Y. S. Edwards, L. M. Sutherland, J. H. T. Power, T. E. Nicholas, and A. W. Murray, FEBS Lett. **448**, 127 (1999).
[17]H. R. Wirtz and L. G. Dobbs, Science **250**, 1266 (1990).
[18]K. J. Cavanaugh, J. Oswari, and S. S. Margulies, Am. J. Respir. Cell Mol. Biol. **25**, 584 (2001).
[19]R. Harding and S. B. Hooper, J. Appl. Physiol. **81**, 209 (1996).
[20]L. Bocconi, C. Boschetto, F. Ceriani, and A. Kustermann, *Development of Normal Fetal Movements* (Springer Milan, 2010), pp. 39–47.
[21]A. Lacoius-Petruccelli, *Perinatal Asphyxia* (Springer, 1987), pp. 97–99.
[22]J. S. Wigglesworth and R. Desai, Lancet **319**, 264 (1982).
[23]S. B. Hooper and R. Harding, J. Appl. Physiol. **69**, 127 (1990).
[24]H. C. Yalcin, S. F. Perry, and S. N. Ghadiali, J. Appl. Physiol. **103**, 1796 (2007).
[25]D. Huh, H. Fujioka, Y.-C. Tung, N. Futai, R. Paine, J. B. Grotberg, and S. Takayama, Proc. Natl. Acad. Sci. U.S.A. **104**, 18886 (2007).
[26]N. J. Douville, P. Zamankhan, Y.-C. Tung, R. Li, B. L. Vaughan, C.-F. Tai, J. White, P. J. Christensen, J. B. Grotberg, and S. Takayama, Lab Chip **11**, 609 (2011).
[27]S. K. Mahto, J. Tenenbaum-Katan, A. Greenblum, B. Rothen-Rutishauser, and J. Sznitman, Am. J. Physiol. **306**, L672 (2014).
[28]A. A. Hislop, J. S. Wigglesworth, and R. Desai, Early Hum. Dev. **13**, 1 (1986).
[29]A. A. Hislop, J. Anat. **201**(14), 325–334 (2002).
[30]P. H. Burri, Biol. Neonate **89**, 313 (2006).
[31]M. DiMaio, J. Gil, D. Ciurea, and M. Kattan, Pediatr. Res. **26**, 88 (1989).
[32]C. Langston, K. Kida, M. Reed, and W. Thurlbeck, Am. Rev. Respir. Dis. **129**, 607 (1984).
[33]A. Tsuda, F. S. Henry, and J. P. Butler, J. Appl. Physiol. **79**, 1055 (1995).
[34]J. Sznitman, J. Biomech. **46**, 284 (2013).
[35]A. Tsuda, F. S. Henry, and J. P. Butler, *Comprehensive Physiology* (John Wiley & Sons, Inc., 2011).
[36]M. Semmler-Behnke, W. G. Kreyling, H. Schulz, S. Takenaka, J. P. Butler, F. S. Henry, and A. Tsuda, Proc. Natl. Acad. Sci. U.S.A. **109**, 5092 (2012).
[37]S. Kumar Mahto, J. Tenenbaum-Katan, and J. Sznitman, Scientifica **2012**, 364054.
[38]D. Huh, B. D. Matthews, A. Mammoto, M. Montoya-Zavala, H. Y. Hsin, and D. E. Ingber, Science **328**, 1662 (2010).
[39]D. D. Nalayanda, C. Puleo, W. B. Fulton, L. M. Sharpe, T.-H. Wang, and F. Abdullah, Biomed. Microdevices **11**, 1081 (2009).
[40]D. C. Duffy, J. C. McDonald, O. J. A. Schueller, and G. M. Whitesides, Anal. Chem. **70**, 4974 (1998).
[41]R. Fishler, M. K. Mulligan, and J. Sznitman, Microfluid. Nanofluid. **15**, 491 (2013).
[42]C. D. Meinhart, S. T. Wereley, and J. G. Santiago, J. Fluids Eng. **122**, 285 (2000).
[43]A. D. Lehmann, N. Daum, M. Bur, C.-M. Lehr, P. Gehr, and B. M. Rothen-Rutishauser, Eur. J. Pharm. Biopharm. **77**, 398 (2011).
[44]K. A. Wikenheiser, D. K. Vorbroker, W. R. Rice, J. C. Clark, C. J. Bachurski, H. K. Oie, and J. A. Whitsett, Proc. Natl. Acad. Sci. U.S.A. **90**, 11029 (1993).
[45]M. Lieber, G. Todaro, B. Smith, A. Szakal, and W. Nelson-Rees, Int. J. Cancer **17**, 62 (1976).
[46]E. R. Weibel, *Morphometry of the Human Lung* (Springer, 1963).
[47]E. S. Boyce, G. S. Dawes, J. D. Gough, and E. R. Poore, Br. Med. J. **2**, 17 (1976).
[48]A. A. Hislop and S. G. Haworth, Am. J. Respir. Crit. Care Med. **140**, 1717 (1989).
[49]D. D. Nalayanda, C. M. Puleo, W. B. Fulton, T.-H. Wang, and F. Abdullah, Exp. Lung Res. **33**, 321 (2007).
[50]J. Sznitman, F. Heimsch, T. Heimsch, D. Rusch, and T. Roüsgen, J. Biomech. Eng. **129**, 658 (2007).
[51]P. Hofemeier and J. Sznitman, J. Biomech. Eng. **136**, 061007 (2014).
[52]J. D. Anderson, *Computational Fluid Dynamics: The Basics with Applications* (McGraw-Hill, New York, 1995).
[53]P. N. Shankar and M. D. Deshpande, Annu. Rev. Fluid Mech. **32**, 93 (2000).
[54]G. Leneweit and D. Auerbach, J. Fluid Mech. **387**, 129 (1999).
[55]B. Ma, V. Ruwet, P. Corieri, R. Theunissen, M. Riethmuller, and C. Darquenne, J. Aerosol Sci. **40**, 403 (2009).
[56]C. van Ertbruggen, P. Corieri, R. Theunissen, M. L. Riethmuller, and C. Darquenne, J. Biomech. **41**, 399 (2008).
[57]H. Kumar, M. H. Tawhai, E. A. Hoffman, and C.-L. Lin, J. Biomech. **42**, 1635 (2009).
[58]J. Sznitman, T. Heimsch, J. H. Wildhaber, A. Tsuda, and T. Rosgen, J. Biomech. Eng. **131**, 031010 (2009).
[59]A. M. Bilek, K. C. Dee, and D. P. Gaver, J. Appl. Physiol. **94**, 770 (2003).
[60]P. J. Hung, P. J. Lee, P. Sabounchi, R. Lin, and L. P. Lee, Biotechnol. Bioeng. **89**, 1 (2005).
[61]N. A. Stathopoulos and J. D. Hellums, Biotechnol. Bioeng. **27**, 1021 (1985).
[62]L. Kim, Y.-C. Toh, J. Voldman, and H. Yu, Lab Chip **7**, 681 (2007).
[63]J. E. Nichols, J. A. Niles, S. P. Vega, L. B. Argueta, A. Eastaway, and J. Cortiella, Exp. Biol. Med. **239**, 1135 (2014).
[64]K. A. Foster, C. G. Oster, M. M. Mayer, M. L. Avery, and K. L. Audus, Exp. Cell Res. **243**, 359 (1998).
[65]M. J. D. Clift, P. Gehr, and B. Rothen-Rutishauser, Arch. Toxicol. **85**, 723 (2011).
[66]H. Tavana, P. Zamankhan, P. J. Christensen, J. B. Grotberg, and S. Takayama, Biomed. Microdevices **13**, 731 (2011).
[67]M. Felder, A. O. Stucki, J. D. Stucki, T. Geiser, and O. T. Guenat, Integr. Biol. **6**, 1132 (2014).
[68]F. Blank, B. M. Rothen-Rutishauser, S. Schurch, and P. Gehr, J. Aerosol Med. **19**, 392 (2006).
[69]K. L. Sellgren, E. J. Butala, B. P. Gilmour, S. H. Randell, and S. Grego, Lab Chip (2014).

[70]A. O. Stucki, J. D. Stucki, S. Hall, M. Felder, Y. Mermoud, R. A. Schmid, T. Geiser, and O. T. Guenat, "A lung-on-a-chip array with an integrated bio-inspired respiration mechanism," Lab Chip (published online 3 December 2014).
[71]C.-M. Lehr, *Cell Culture Models of Biological Barriers: In Vitro Test Systems for Drug Absorption and Delivery* (CRC Press, 2003).
[72]S. K. Mahto, V. Charwat, P. Ertl, B. Rothen-Rutishauser, S. W. Rhee, and J. Sznitman, Nanotoxicology **2014**, 1.
[73]B. M. Rothen-Rutishauser, S. G. Kiama, and P. Gehr, Am. J. Respir. Cell Mol. Biol. **32**, 281 (2005).
[74]B. Haefeli-Bleuer and E. R. Weibel, Anat. Rec. **220**, 401 (1988).
[75]R. Lima, S. Wada, K. Tsubota, and T. Yamaguchi, Meas. Sci. Technol. **17**, 797 (2006).
[76]See supplementary material at http://dx.doi.org/10.1063/1.4908269 for detailed derivation of wall shear stress values in our model and additional data on computational simulations as well as model limitations.